Inorg. Chem. **2006**, *45*, 3803–3815

CO_2 Fixation by Cu^{2+} and Zn^{2+} Complexes of a Terpyridinophane Aza Receptor. Crystal Structures of Cu^{2+} Complexes, pH-Metric, Spectroscopic, and Electrochemical Studies

Begoña Verdejo, Juan Aguilar, and Enrique García-España*

Departamento de Química Inorgánica, Instituto de Ciencia Molecular, Universidad de Valencia, Edificio de Institutos de Paterna, Apartado de Correos 22085, 46071 Valencia, Spain

Pablo Gaviña

Departamento de Química Orgánica, Instituto de Ciencia Molecular, Universidad de Valencia, Edificio de Institutos de Paterna, Apartado de Correos 22085, 46071 Valencia, Spain

Julio Latorre

Departamento de Química Inorgánica, Instituto de Materiales de la Universidad de Valencia, Universidad de Valencia, C/Dr. Moliner 46100, Burjassot, Valencia, Spain

Conxa Soriano and José M. Llinares

Departamento de Química Orgánica, Instituto de Ciencia Molecular, Facultad de Farmacia, Universidad de Valencia, Avda. Vicente Andrés Estellés s/n, 46100, Burjassot, Valencia, Spain

Antonio Doménech

Departamento de Química Analítica, Universidad de Valencia, C/Dr. Moliner 46100, Burjassot, Valencia, Spain

Received February 17, 2006

The synthesis of the terpyridinophane-type polyamine 2,6,9,12,16-pentaaza[17]-(5,5′′)-cyclo-(2,2′:6′,2′′)-terpyridinophane heptahydrobromide tetrahydrate (**L**·7HBr·4H_2O) is described. **L** presents six protonation constants with values in the range 9.21–3.27 logarithmic units. **L** interacts with Cu^{2+} and Zn^{2+} forming in both cases, neutral, protonated, and hydroxylated mono- and binuclear complexes whose constants have been calculated by potentiometry in 0.15 M $NaClO_4$ at 298.1 K. The crystal structures of the compounds [Cu(H**L**-carb)(H_2O)](ClO_4)$_3$·2H_2O (**1**) and [Cu_2(H_2**L**)(CO_3)]$_2$(ClO_4)$_8$·9H_2O (**2**) have been solved by X-ray diffraction. In **1**, the metal center presents square pyramidal geometry. The base of the pyramid is formed by the three nitrogen atoms of pyridine and one oxygen atom of a CO_2 group which is forming a carbamate bond with the central nitrogen atom of the polyamine chain. The axial position is occupied by a water molecule. In **2**, one Cu^{2+} is bound by the three pyridine nitrogens and the other one by the three central nitrogen atoms of the polyamine chain. The square planar coordination geometry is completed by a carbonate group taken up from the atmosphere that behaves as a bridging μ,μ'-ligand between the two centers. The pH-metric titrations on the ternary Cu^{2+}–**L**–carbonate and Zn^{2+}–**L**–carbonate systems show the extensive formation of adduct species which above pH 6 are formed quantitatively in solution. The stoichiometries of the main species formed in solution at pH = 6.8 agree with those found in the crystalline compounds. CO_2 uptake by the Zn^{2+} and Cu^{2+} 1:1 complexes in aqueous solution has also been followed by recording the variations in the band at ca. 300 nm. The formation of the Zn^{2+} carbamate moiety has been evidenced by ^{13}C NMR and ESI spectroscopy.

Introduction

Very often, biological processes are assisted by amino groups that fix or react with a given compound. A paramount example of such chemistry comes from the most abundant enzyme in nature, rubisco, which participates in the fixation of CO_2 by green plants through the formation of a carbamate moiety by reaction of CO_2 and a lysine side chain assisted by Mg^{2+} or Mn^{2+} ions.[1] The elusive carbamate moiety is

* To whom correspondence should be addressed. E-mail: enrique.garcia-es@uv.es.

10.1021/ic060278d CCC: $33.50
Published on Web 03/28/2006

Chart 1

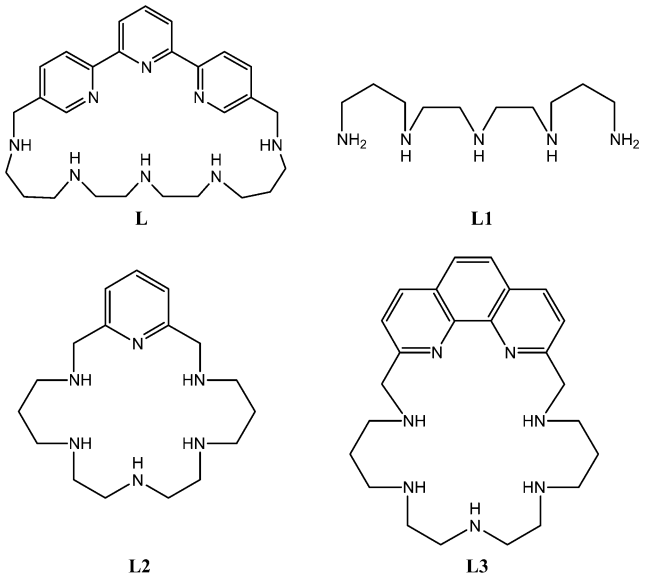

further stabilized by formation of a hydrogen-bond network with other amino acid residues.

In the last years some of us have concentrated our efforts in the study of the coordination chemistry of [1 + 1] azacyclophane molecules containing different aromatic spacers and donor atoms.[2] The goal was to generate coordinatively unsaturated metal sites, which could bind different substrates through the formation of ternary complexes occupying the vacant positions in the coordination sphere or by removing the labile ancillary ligands that would be completing the coordination spheres of the metal ions. In this context, in a previous study some of us have evidenced the capacity of the copper(II) and zinc(II) complexes of a couple of cyclophanes containing *m*- or *p*-xylene spacers to interact with hydrogencarbonate or carbonate in aqueous solution.[2c]

Following these ideas we had recently incorporated in our [1 + 1] cyclophane ligands the polyamine 1,5,8,11,15-pentaazapentadecane (**L1**) connected through methylene groups to a 2,6-pyridine spacer (**L2**, Chart 1).[3] The point was to achieve the coordination of one metal ion even if the polyamine chain had several protonated nitrogen donors. However, in the case of this macrocycle, its size and flexibility permit the involvement of all the nitrogen atoms in the coordination to the metal. This would prevent the uptake of further molecules without breaking any of the metal−nitrogen bonds. Thus, a further step to attain simultaneous metal ion and CO_2 fixation was the introduction of the rigid bidentate ligand phenanthroline as a spacer (**L3** in Chart 1).[4,5] The idea would be to retain the metal ion in the bidentate fragment, leaving free the polyamine chain for CO_2 fixation. However, in this case, the metal ion can move from the phenanthroline site to the polyamine site in response to pH changes,[5] handicapping CO_2 uptake (vide infra). Therefore, to block more firmly the metal ion at one side of the molecule, we have now introduced as spacer the tridentate moiety 2,2′:6′,2″-terpyridine connected at its 5,5″ positions to the polyamine bridge to give ligand **L** (Chart 1). (The crystal structures of **1** and **2** and some preliminary studies in solutions have been advanced in ref 22b.)

Terpyridine has been used as a ligand by itself and as building block of a variety of supramolecular metal assemblies because of its capacity for fitting three corners of a polyhedron.[6] Also in a few cases terpyridine has been used as an integral part of azacyclophane structures.[7]

Here we report on the synthesis and protonation behavior of **L** as well as on its capacity to bind the metal ions Cu^{2+} and Zn^{2+}. In addition, we have analyzed their ability to incorporate atmospheric CO_2. We compare these results with those obtained with the open-chain polyamine **L1** and with the analogous ligands containing phenanthroline (**L3**) and pyridine (**L2**) as spacers (see Chart 1).

Experimental Section

5,5″-Dimethyl-2,2′:6′,2″-terpyridine (**3**),[8] 5,5″-bis(bromomethyl)-2,2′:6′,2″-terpyridine (**4**),[9] and 1,5,8,11,15-pentakis(*p*-tolylsulfonyl)-1,5,8,11,15-pentaazapentadecane (**5**)[10] were prepared as described previously. The other chemicals were used as purchased without further purification. CH_3CN was dried over 3 Å molecular sieves. CH_2Cl_2 was distilled from CaH_2 prior to its use. Column chromatography was performed with aluminum oxide (neutral, SDS). Aluminum oxide 60 F_{254} neutral (Merck) plates were used for TLC.

(1) Cleland, W. W.; Andrews, T. J.; Gutteridge, S.; Hartman, F. C.; Lorimer, G. H. *Chem. Rev.* **1998**, *98*, 549−561.
(2) (a) Aguilar, J. A.; García-España, E.; Guerrero, J. A.; Luis, S.V.; Llinares, J. M.; Ramírez J. A.; Soriano, C. *J. Chem. Soc. Chem. Commun.* **1995**, 2237−2239. (b) Burguete, M. I.; Díaz, P.; García-España, E.; Luis, S. V.; Miravet, J. F.; Querol, M.; Ramírez, J. A. *Chem. Commun.* **1999**, 649−650. (c) Andrés, S.; Escuder, B.; Doménech, A.; García-España, E.; Luis, S.V.; Marcelino, V.; Llinares, J. M.; Ramírez J. A.; Soriano, C. *J. Phys. Org. Chem.* **2001**, *14*, 495−500.
(3) Díaz, P.; Basallote, M. G.; Máñez, M. A.; García-España, E.; Gil, L.; Latorre, J.; Soriano, C.; Verdejo, B.; Luis, S. V. *J. Chem. Soc., Dalton Trans.* **2003**, 1186−1193.
(4) Aguilar, J.; Bencini, A.; Berni, E.; Bianchi, A.; García-España, E.; Gil, L.; Mendoza, A.; Ruiz-Ramírez, L.; Soriano, C. *Eur. J. Inorg. Chem.* **2004**, 4061−4071.
(5) Mendoza, A.; Aguilar, J.; Basallote, M. G.; Gil, L.; Hernández, J. C.; Máñez, M. A.; García-España, E.; Soriano, C.; Ruiz-Ramírez, L.; Verdejo, B. *Chem. Commun.* **2003**, 3032−3033.
(6) (a) Hasenknopf, B.; Lehn, J.-M.; Baum, G.; Fenske, D. *Proc. Natl. Acad. Sci. U.S.A.* **1996**, *93*, 1397−1400. (b) Constable, E. C.; Kulke, T.; Newburger, M.; Zehnder, M. *Chem. Commun.* **1997**, 489−490. (c) Harriman, A.; Ziessel, R. *Coord. Chem. Rev.* **1998**, *171*, 331−339. (d) Newkome, G. R.; Cho, T. J.; Moorefield, C. N.; Baker, J. R.; Saunders, M. J.; Cush, R.; Russo, P. S. *Angew. Chem., Int. Ed.* **1999**, *38*, 3717−3721. (e) Collin, J.-P.; Dietrich-Buchecker, C.; Gaviña, P.; Jiménez-Molero, M. C.; Sauvage, J.-P. *Acc. Chem. Res.* **2001**, *34*, 477−487.
(7) (a) Constable, E. C.; Holmes, J. H. *Polyhedron* **1988**, 7, 2531−2536. (b) Márquez, V. E.; Anacona, J. R.; Rodriguez Barbarin, C. *Polyhedron* **2001**, *20*, 1885−1890. (c) Galaup, C.; Couchet, J. M.; Picard, C.; Tisnès, P. *Tetrahedron Lett.* **2001**, 6275−6278. (d) Baxter, P. N. W. *Chem.−Eur. J.* **2003**, *9*, 5011−5022. (e) Wong, W.-L.; Huang, K.-H.; Teng, P.-F.; Lee, C.-S.; Kwong H−L. *Chem. Commun.* **2004**, 384−385. (f) Bazzicalupi, C.; Bencini, A.; Berni, E.; Bianchi, A.; Danesi, A.; Giorgi, C.; Valtancoli, B.; Lodeiro, C.; Lima, J. C.; Pina, F.; Bernardo, M. A. *Inorg. Chem.* **2004**, *43*, 5134−5146. (g) Bazzicalupi, C.; Bencini, A.; Bianchi, A.; Danesi, A.; Giorgi, C.; Lodeiro, C.; Pina, F.; Santarelli, S.; Valtancoli, B. *Chem. Commun.* **2005**, 2630−2362.
(8) Cárdenas, D. J.; Sauvage, J.-P. *Synlett* **1996**, 916−918 and references therein.
(9) Jimenez-Molero, M. C.; Dietrich-Buchecker, C.; Sauvage, J.-P. *Chem.−Eur. J.* **2002**, *8*, 1456−1466.
(10) Aguilar, J. A.; Díaz, P.; Escartí, F., García-España, E.; Gil, L.; Soriano, C.; Verdejo, B. *Inorg. Chim. Acta* **2002**, *339*, 307−316.

2,6,9,12,16-Pentakis(*p*-tolylsulfonyl)-2,6,9,12,16-pentaaza[17]-(5,5″)-cyclo-(2,2′:6′,2″)-terpyridinophane (L·5Ts). 5,5″-Bis(bromomethyl)-2,2′:6′,2″-terpyridine (**4**) (0.33 g, 0.78 mmol) in dry CH_2Cl_2 (30 mL) was slowly added dropwise over a mixture of **5** (0.77 g, 0.78 mmol) and K_2CO_3 (1.08 g, 7.8 mmol) in refluxing CH_3CN (55 mL). Once the addition was over, most of the CH_2Cl_2 was distilled, and the resulting mixture was refluxed under argon for 20 h. Then the solution was filtered through paper while hot, as the solid was washed thoroughly with more CH_3CN. The combined organic layers were concentrated in vacuo to give an orange solid (1.12 g) which was submitted to column chromatography (Al_2O_3, CH_2Cl_2 with 0−5% AcOEt as eluent) to afford **L·**5Ts (0.48 g, 49%) as a white solid. ^{1}H NMR ($CDCl_3$, 300 MHz), δ_H (ppm): 8.95 (d, J = 8.3 Hz, 2H), 8.50 (d, J = 2.1 Hz, 2H), 8.39 (d, J = 7.8 Hz, 2H), 8.19 (dd, J = 8.3 and 2.1 Hz, 2H), 7.94 (t, J = 7.8 Hz, 1H), 7.78 (d, J = 8.3 Hz, 4H), 7.73 (d, J = 8.3 Hz, 2H), 7.58 (d, J = 8.3 Hz, 4H), 7.42−7.36 (m, 6H), 7.16 (d, J = 8.3 Hz, 4H), 4.28 (br s, 4H), 3.11−2.98 (m, 8H), 2.98−2.88 (m, 4H), 2.86−2.75 (m, 4H), 2.47 (s, 6H), 2.45 (s, 3H), 2.33 (s, 6H), and 1.50−1.40 (m, 4H). ^{13}C NMR ($CDCl_3$), δ_C (ppm): 156.7, 155.1, 149.1, 144.3, 143.7, 138.6, 135.5, 132.9, 130.6, 130.4, 130.3, 127.8, 127.6, 127.4, 122.7, 121.1, 52.8, 48.3, 47.6, 47.3, 22.0, 21.8. HRMS (FAB): calcd for $C_{62}H_{69}N_8O_{10}S_5$ (MH^+), 1245.374; found, 1245.378.

2,6,9,12,16-Pentaaza[17]-(5,5″)-cyclo-(2,2′:6′,2″)-terpyridinophane Heptahydrobromide Tetrahydrate (L·7HBr·4H_2O). L·5Ts (0.336 g, 0.27 mmol) and phenol (1.60 g, 17.1 mmol) were dissolved in 20 mL of 33% HBr/HAc, and the mixture was heated at 90 °C with stirring for 24 h. The solid obtained was filtered off and washed with a mixture of EtOH/CH_2Cl_2 (1:1). The macrocycle was obtained as its hydrobromide salt (0.240 g, 97%). ^{1}H NMR (D_2O), δ_H (ppm): 9.11 (d, J = 1.7 Hz, 2H), 8.69 (d, J = 8.5 Hz, 2H), 8.59 (dd, J = 8.5 and 1.7 Hz, 2H), 8.56−8.43 (m, 3H), 4.67 (s, 4H), 3.49 (br.s, 8H), 3.27−3.16 (m, 8H) and 2.18−2.10 (m, 4H). ^{13}C NMR (D_2O), δ_C (ppm): 153.2, 151.6, 148.7, 143.7, 128.0, 124.4, 124.2, 47.3, 44.9, 43.1, 42.9, 42.6, 22.5. Anal. Calcd for $C_{27}H_{38}N_8$·7HBr·4H_2O: C, 29.1; H, 4.8; N, 10.1. Found: C, 29.3; H, 4.6; N, 9.8.

Materials and Methods. EMF Measurements. The potentiometric titrations were carried out at 298.1 ± 0.1 K using 0.15 M $NaClO_4$ as supporting electrolyte. The experimental procedure (buret, potentiometer, cell, stirrer, microcomputer, etc.) has been fully described elsewhere.[11] The acquisition of the emf data was performed with the computer program PASAT.[12] The reference electrode was a Ag/AgCl electrode in saturated KCl solution. The glass electrode was calibrated as a hydrogen-ion concentration probe by titration of previously standardized amounts of HCl with CO_2-free NaOH solutions and the equivalent point determined by the Gran's method,[13] which gives the standard potential, $E^{o\prime}$, and the ionic product of water (pK_w = 13.73(1)).

The computer program HYPERQUAD was used to calculate the protonation and stability constants.[14] The pH range investigated was 2.5−11.0, and the concentration of the metal ions and of the ligands ranged from 1×10^{-3} to 5×10^{-3} M with M/**L** molar ratios varying from 2:1 to 1:2. For the ternary systems, aqueous solutions at basic pH containing M/**L** in 1:1 and 2:1 molar ratios and different amounts of Na_2CO_3 were titrated with $HClO_4$ solutions. The different titration curves for each system (at least two) were treated either as a single set or as separated curves without significant variations in the values of the stability constants. Finally, the sets of data were merged together and treated simultaneously to give the final stability constants.

NMR Measurements. The ^{1}H and ^{13}C NMR spectra were recorded on a Bruker Advance AC-300 spectrometer operating at 299.95 MHz for ^{1}H and at 75.43 for ^{13}C. For the ^{13}C NMR spectra, dioxane was used as a reference standard (δ = 67.4 ppm), and for the ^{1}H spectra, the solvent signal was used.

Adjustments to the desired pH were made using drops of DCl or NaOD solutions. The pD was calculated from the measured pH values using the correlation, pH = pD − 0.4.[15]

Spectrophotometric Titrations. Absorption spectra were recorded on a Shimadzu UV-2501PC spectrophotometer. HCl and NaOH were used to adjust the pH values that were measured on a Meterlab PHM240 radiometer pH meter.

ESI Mass Spectroscopy. ESI-MS spectra were recorded with an Esquire 300 (Bruker) by electrospray positive mode (ES^+).

Electrochemical Measurements. Linear potential scan, cyclic, and square wave voltammetric experiments (LSV, CV, and SQWV, respectively) were performed on aqueous solutions (0.15 M $NaClO_4$) of $Cu(NO_3)_2$ (Merck) and $Zn(NO_3)_2$ (Merck) in 10^{-3} M concentration containing a stoichiometric amount or a small excess of each one of the macrocyclic ligands. For the study of the electrochemistry of binary metal-macrocycle complexes, equimolar amounts of metal nitrate and the ligand were dissolved in 0.15 M $NaClO_4$, previously degassed with argon, and then voltammograms were recorded. To study ternary M−**L**−carbonate complexes, the metal-receptor solution was exposed to air by stirring for 30 min to 6 h; the resulting solution was then degasified by bubbling argon for 10 min, and then the voltammograms were recorded.

The pH was adjusted to the required values by adding appropriate amounts of aqueous HCl and/or NaOH solutions.

Electrochemical experiments were performed with BAS CV 50W and CH I420 equipment in a conventional three-compartment cell with glassy-carbon and gold working electrodes. Prior to series of experiments, the working electrode was cleaned and activated. Electrochemical pretreatment was performed, by adapting the procedure recommended by Engstrom and Strasser,[16] in blank solutions by applying +1.50 V vs AgCl/Ag for 10 min followed by −1.0 V for 1 min. Before each run the electrodes were polished with an aqueous suspension of alumina on a soft surface, dried, and cleaned. An AgCl (3 M NaCl)/Ag and a platinum wire auxiliary electrode completed the three electrode configuration. Eventually semiderivative convolution of data was used to increase peak resolution.

Electrochemical quartz crystal microbalance experiments (EQCM) were performed with CH I420 equipment using a gold-coated AT-cut quartz crystal. The quartz crystal and gold electrodes have diameters of 1.20 and 0.50 cm, respectively. The reference and counter electrodes were the same as in voltammetric studies. The EQCM instrument was calibrated via electrochemical deposition of copper from 10 mM $Cu(ClO_4)_2$ + 0.10 M $HClO_4$ following the procedure described by Deakin and Melroy.[17] Assumptions associ-

(11) García-España, E.; Ballester, M. J.; Lloret, F.; Moratal, J. M.; Faus, J.; Bianchi, A. *J. Chem. Soc., Dalton Trans.* **1988**, 101−104.
(12) Fontanelli, M.; Micheloni, M. Program for the Automatic Control of the Microburet and the Acquisition of the Electromotive Force Readings. Proceedings of the I Spanish−Italian Congress on Thermodynamics of Metal Complexes, Peñíscola, Castellón, Spain, 1990.
(13) (a) Gran, G. *Analyst (London, U.K.)* **1952**, *77*, 661−663. (b) Rossotti, F. J.; Rossotti, H. *J. Chem. Educ.* **1965**, *42*, 375−378.
(14) Gans, P.; Sabatini, A.; Vacca, A. *Talanta* **1996**, *43*, 1739−1753.
(15) Covington, A. K.; Paabo, M.; Robinson, R. A.; Bates. R. G. *Anal. Chem.* **1968**, *40*, 700−710.
(16) Engstrom, R. C.; Strasser, V. A. *Anal. Chem.* **1984**, *56*, 136−141.
(17) Deakin, M. R.; Melroy, O. *J. Electroanal. Chem.* **1988**, *239*, 321−331.

Scheme 1 [a]

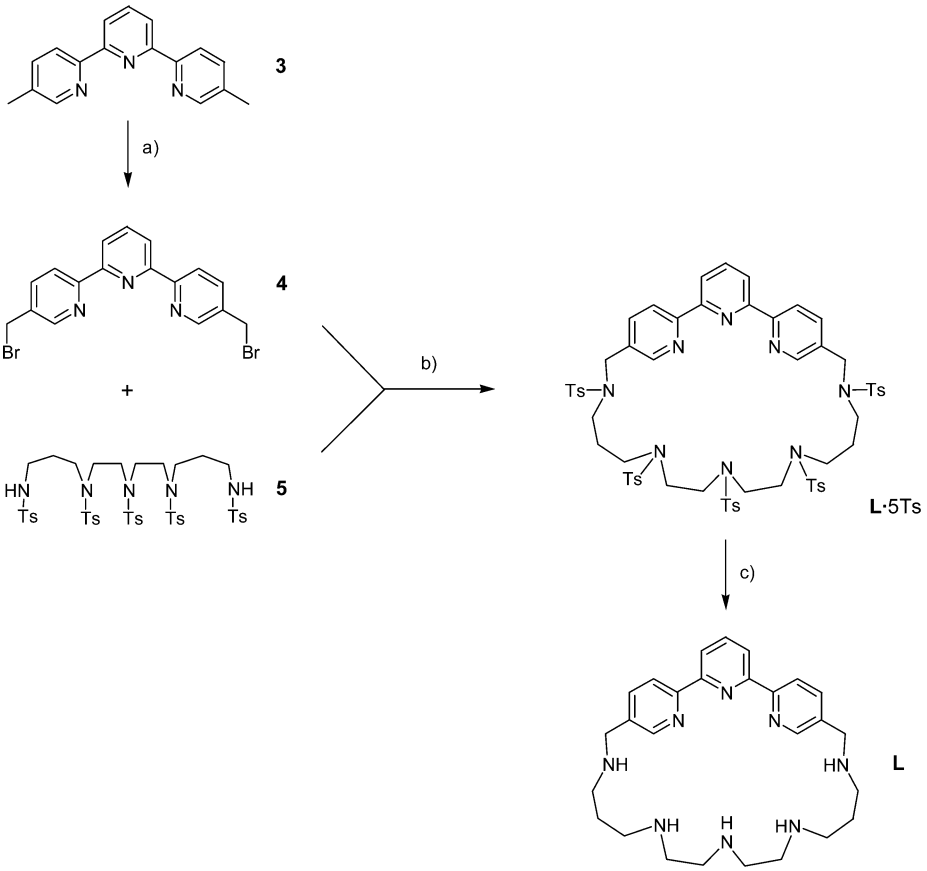

[a] Reagents and conditions: (a) NBS, benzene, reflux, *hν* (45%); (b) K_2CO_3, CH_3CN, reflux (49%); (c) HBr/HOAc, PhOH, reflux (97%).

ated with the use of the Sauerbrey equation to determine mass changes were as described by Bond et al.[18]

Crystallographic Analyses. Blue crystals of **1** suitable for X-ray diffraction analysis were obtained by slow evaporation in an open vessel of aqueous solutions containing $Cu(ClO_4)_2$ and **L** in 1:1 molar ratio with an initial pH of 9. Blue crystals of **2** were obtained by the same procedure but with $Cu(ClO_4)_2$ and **L** in 2:1 molar ratio. The final pH of the solution from which the crystal evolved was in both cases 6.8. Anal. Calcd for $C_{28}H_{45}N_8Cl_3O_{17}Cu$ (**1**): C, 35.94; H, 4.84; N, 11.98. Found: C, 35.6; H, 4.64; N, 11.8. Anal. Calcd for $C_{56}H_{98}N_{16}Cl_8O_{47}Cu_4$ (**2**): C, 29.43; H, 4.32; N, 9.81. Found: C, 29.3; H, 4.4; N, 9.8.

Analysis on single crystals of the ligand was carried out with an Enraf-Nonius KAPPA CCD single-crystal diffractometer (λ = 0.710 73 Å). The space groups were $P2_{1/c}$ and $P2_1$ for **1** and **2**, respectively. A total of 2497 and 11 570 reflections were measured in the *hkl* range (−15, −7, −24) to (15, 4, 24) and (−17, −13, −23) to (17, 14, 23) between θ limits 2.68° < θ < 45.28° and 1.70° < θ < 23.30° for **1** and **2**, respectively. The structure was solved by the Patterson method using the program SHELXS-86,[19] running on a Pentium 100 computer. Isotropic least-squares refinement was performed by means of the program SHELXL-93.[20] Some of the hydrogen atoms were located in the electron density map, and the rest of them were geometrically fixed. Crystal data, data collection parameters, and results of the analyses are listed in Table 1. Data for **1** were collected at 293(2) K, and data for **2** were collected at 150(2) K because disorder was found within the perchlorate counteranions.

Table 1. Crystallographic Data for [Cu(H**L**-carb)(H_2O)](ClO_4)$_3$·2H_2O (**1**) and [Cu_2(H_2**L**)(CO_3)]$_2$(ClO_4)$_8$·9H_2O (**2**)

	1	**2**
empirical formula	$C_{28}H_{45}N_8O_{17}Cl_3Cu$	$C_{56}H_{98}N_{16}O_{47}Cl_8Cu_4$
fw	935.62	2285.20
cryst size, mm	0.1 × 0.05 × 0.1	0.1 × 0.1 × 0.15
cryst syst, space group	monoclinic, $P2_{1/c}$	monoclinic, $P2_1$
T, K	293(2)	150(2)
a, Å	17.9720(8)	15.7820(7)
b, Å	8.4000(3)	13.2970(6)
c, Å	28.3150(12)	21.1290(12)
α, deg	90	90
β, deg	113.3070(16)	94.314(2)
γ, deg	90	90
V, Å^3	3925.8(3)	4421.43(7)
Z	4	4
d_{calcd}, g/cm^3	1.573	1.641
μ, mm^{-1}	0.822	1.290
reflns collected	3800	11570
unique reflns	2497	11570
restraints	39	1
params	556	889
R1, wR2 (all)	0.0782, 0.1922	0.0749, 0.215
GOF	1.347	1.191

During the final stages of the refinement the positional parameters and the anisotropic thermal parameters of the non-hydrogen atoms were refined. The hydrogen atoms were refined with a common thermal parameter. Atomic scattering factors were taken from ref 20. Molecular plots were produced with the program ORTEP.[21]

(18) Bond, A. M.; Miao, W.; Raston, C. L. *J. Phys. Chem. B* **2000**, *104*, 2320−2329.
(19) Sheldrick, G. M., Kruger, C., Goddard, R., Eds. *Crystallographic Computing;* Clarendon Press: Oxford, England, 1985; p 175.
(20) Sheldrick, G. M. *SHELXL-93: Program for Crystal Structure Refinement;* Institut für Anorganische Chemie, University of Göttingen: Göttingen, Germany, 1993.
(21) Johnson, C. K. *ORTEP: Report ORNL-3794;* Oak Ridge National Laboratory: Oak Ridge, TN, 1971.

Table 2. Protonation Constants of the Receptors **L**, **L1**, **L2**, and **L3** Determined in 0.15 M $NaClO_4$ at 298.1 K

entry	reaction	**L**	**L1**[d]	**L2**[e]	**L3**[f]
1	$\mathbf{L} + H = \mathbf{L}H$ [a]	9.21(1)[b]	10.55	9.65	10.01
2	$\mathbf{L}H + H = \mathbf{L}H_2$	8.17(3)	9.89	9.32	9.15
3	$\mathbf{L}H_2 + H = \mathbf{L}H_3$	7.04(3)	8.69	7.62	7.81
4	$\mathbf{L}H_3 + H = \mathbf{L}H_4$	5.74(4)	7.55	6.62	6.42
5	$\mathbf{L}H_4 + H = \mathbf{L}H_5$	3.82(4)	3.55	2.86	2.97
6	$\mathbf{L}H_5 + H = \mathbf{L}H_6$	3.27(4)			
7	$\log \beta$[c]	37.25	40.20	36.10	36.36

[a] Charges omitted for clarity. [b] Values in parentheses are standard deviations in the last significant figure. [c] Global basicity constant $\beta = (\sum K_{HjL})$. [d] Taken from ref 23. [e] Taken from ref 3. [f] Taken from ref 5.

Results and Discussion

Synthesis. The synthesis of **L** is sketched in Scheme 1. 5,5″-Dimethyl-2,2′:6′,2″-terpyridine (**3**) was prepared from 2,6-dibromopyridine and tributyl(5-methylpyridin-2-yl)stannane by a double Stille cross-coupling reaction.[8]

Irradiation of a mixture of **3** and *N*-bromosuccinimide in refluxing benzene gave the dibromo derivative **4** in 46% yield.[9] Cyclization of **4** with the pentakis(*p*-tolylsulfonyl)-polyamine **5**[10] in the presence of K_2CO_3 as a base, in refluxing CH_3CN, yielded **L**·5Ts as a white solid in 49% yield after column chromatography. Finally, the tosyl groups of **L**·5Ts were removed by reductive cleavage with a mixture of HBr/AcOH and PhOH at 90 °C,[22a] affording the terpyridine-containing polyazacyclophane **L** as its hydrobromide salt (**L**·7HBr) in 97% yield.[22b]

Protonation Constants. Table 2 collects the stepwise protonation constants of **L** along with those previously reported for cyclophane receptors **L2** and **L3** and the open-chain polyamine **L1**, determined in 0.15 M $NaClO_4$ at 298.1 K. The distribution diagram of the species existing throughout the pH range 2.0−11.0 is shown in the Supporting Information (Figure S1).

Differently to macrocycles **L2** and **L3** which just show five stepwise constants that have been ascribed to protonation steps involving the polyamine bridge, **L** presents, in the pH range of the potentiometric study (pH = 2−11), six protonation constants which vary from 9.21 logarithmic units for the first protonation constant to 3.27 for the last one and are lower than those obtained for macrocycles **L2** and **L3** with the pyridine or phenanthroline spacers or for the open-chain polyamine **L1**. This can be explained by the electron withdrawal characteristics of the terpyridine fragment. Such a behavior was also observed for a related terpyridinophane macrocycle substituted at the 6,6″ positions instead of at the 5,5″ positions.[7f]

The extra protonation attained by **L** with respect to **L2** and **L3** should necessarily involve the terpyridine moiety. To decide at which stage occurs the protonation of the terpyridine nitrogens, we have recorded the variation with the pH of the UV−vis spectra of **L**. Figure 1 shows that from pH 10.4 to 3.9 the UV−vis spectrum of **L** does not experience significant variations and consists of two bands

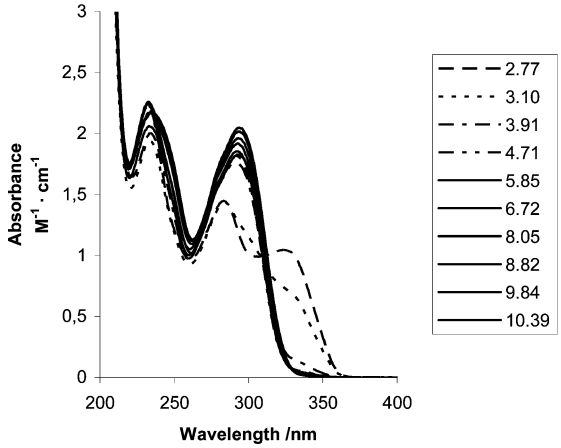

Figure 1. The pH dependence of the absorption spectra of **L**.

centered at 230 (ϵ = 22 084 mol^{-1} dm^3 cm^{-1}) and 290 nm (ϵ = 20 834 mol^{-1} dm^3 cm^{-1}). Below pH 4, the band at 290 nm splits into two giving rise to a bathochromically shifted band centered at 323 nm (ϵ = 10 634 mol^{-1} dm^3 cm^{-1}) and a slightly hypsochromically shifted band at 281 nm (ϵ = 14 686 mol^{-1} dm^3 cm^{-1}).

The initial band at 290 nm would indeed be the result of two overlapped $\pi\pi^*$ transitions whose dipolar moments are oriented along the larger and shorter axes of the terpyridine unit,[24] from which the band with its associated dipolar moment oriented along the shorter axes is more sensitive to the protonation of the terpyridine fragment. Therefore, below pH 4, protonation of the terpyridine fragment produces a bathochromic shift of such a band while the other one slightly shifts hypsochromically. These observations support that protonation of the terpyridine moiety only occurs with the last protonation step.

Cu^{2+} Coordination in Aqueous Solution. In Table 3 are included the formation constants for the system Cu^{2+}−**L** along with those we had previously reported for the macrocycles **L2** and **L3** and the open-chain polyamine **L1**. The studies were carried out at 298.1 K using 0.15 mol dm^{-3} $NaClO_4$ as background electrolyte.

The first point that deserves comment is that in this system there is not strong competition between ligand protonation and Cu^{2+} complex formation equilibria because of the low basicity of **L** and because of the fact that complexes with high protonation degrees are formed at very low pH values. Therefore, to obtain reliable values of the stability constants, it was necessary to perform a large number of titrations with different metal/**L** mole ratios. The number of points fitted were 596, coming from eight different titrations in which the Cu^{2+}/**L** mole ratios varied from 2:1 to 1:2. The speciation showed the formation of $[CuH_x\mathbf{L}]^{(2+x)}$ mononuclear species with x varying between 5 and 0 and of binuclear $[Cu_2H_x\mathbf{L}]^{(4+x)}$ species with x from 2 to −2.

The protonation degree of 5 of the complex formed at lower pH suggests that **L** can coordinate the metal ion

(22) (a) Bencini, A.; Burguete, M. I.; García-España, E.; Luis, S. V.; Miravet, J. F.; Soriano, C. *J. Org. Chem.* **1993**, *58*, 4749−4753. (b) García-España, E.; Gaviña, P.; Latorre, J.; Soriano, C.; Verdejo, B. *J. Am. Chem. Soc.* **2004**, *126*, 5082−5083.

(23) Gampp, H.; Haspra, D.; Maeder, M.; Zuberbuehler, M. *Inorg. Chem.* **1984**, *23*, 3724−3730.

(24) *Hyperchem*, version 6.01 for Windows; Hypercube, Inc.: Gainesville, FL, 2000.

Table 3. Stability Constants for the Formation of Cu^{2+} Complexes for the Receptors **L**, **L1**, **L2**, and **L3** Determined in 0.15 M $NaClO_4$ at 298.1 K

entry	reaction	**L**	**L1**[c]	**L2**[d]	**L3**[e]
1	$M + L \leftrightarrows ML$[a]	~13.1	21.28(2)	20.44(3)	15.98(6)
2	$M + L + H \leftrightarrows MHL$	22.80(5)[b]	30.14(7)	27.40(1)	26.26(5)
3	$M + L + 2H \leftrightarrows MH_2L$	30.18(6)	33.53(1)	30.15(2)	29.9(1)
4	$M + L + 3H \leftrightarrows MH_3L$	36.42(6)			35.09(7)
5	$M + L + 4H \leftrightarrows MH_4L$	41.88(6)			38.48(4)
6	$M + L + 5H \leftrightarrows MH_5L$	45.81(6)			
7	$ML + H \leftrightarrows MHL$	~9.7	8.86(7)	6.96(3)	10.28(6)
8	$MHL + H \leftrightarrows MH_2L$	7.38(1)	3.39(7)	2.75(2)	3.64(5)
9	$MH_2L + H \leftrightarrows MH_3L$	6.23(1)			5.59(7)
10	$MH_3L + H \leftrightarrows MH_4L$	5.46(1)			3.39(8)
11	$MH_4L + H \leftrightarrows MH_5L$	3.93(1)			
12	$2M + L \leftrightarrows M_2L$	25.54(7)			27.5(1)
13	$2M + L + H \leftrightarrows M_2HL$	31.93(7)			
14	$2M + L + H \leftrightarrows M_2HL$	37.34(7)			
15	$M_2L + H \leftrightarrows M_2HL$	6.38(1)			4.1(1)
16	$M_2L + H \leftrightarrows M_2HL$	5.41(2)			
17	$2M + L + H_2O \leftrightarrows M_2L(OH) + H$	18.78 (8)		20.65(2)	18.1(1)
18	$2M + L + 2H_2O \leftrightarrows M_2L(OH)_2 + H$	8.43(8)		10.84(4)	
19	$M_2L + H_2O \leftrightarrows M_2L(OH) + H$	−6.76(2)			−9.4(1)
20	$M_2L(OH) + H_2O \leftrightarrows M_2L(OH)_2 + H$	−10.35(4)		−9.81(5)	

[a] Charges omitted. [b] Values in parentheses are standard deviations in the last significant figure. [c] Taken from ref 10. [d] Taken from ref 3. [e] Taken from ref 5.

exclusively through the terpyridine nitrogens even if all the nitrogens of the polyamine chain are protonated. The values of the constants for the successive protonation steps of $[CuL]^{2+}$ compare favorably with the protonation steps of the free ligand with the same overall charges supporting the latter conclusion (compare for instance, entry 7 in Table 3 and entry 3 in Table 2).

In addition, the value of the constant estimated for the formation of the $[CuL]^{2+}$ complex is much lower than that reported for **L2** in which three nitrogen atoms of the polyamine and the pyridine nitrogen atom were tightly bound in the equatorial positions of a very distorted octahedron which completed the axial positions with the two benzylic nitrogens at a much longer distance.[3] Also, the constant found for the Cu^{2+} complex of **L3** is slightly higher than the one observed for **L**. In the system $Cu^{2+}-$**L3**, a migration of the metal ion from the phenanthroline unit to the central part of the polyamine was identified by spectroscopy and stopped-flow kinetics.[5] In addition, the value for the formation of the $[CuL]^{2+}$ complex is close to the value reported in the literature for the formation of the $[Cu(terpy)]^{2+}$ complex.[25]

Complexation of Cu^{2+} (mole ratio Cu^{2+}/**L** 1:1) yields spectral changes similar to those produced by the protonation of the terpyridine fragment with the appearance of two bands at 330 ($\epsilon = 14\,681$ mol^{-1} dm^3 cm^{-1}) and 340 nm ($\epsilon = 14\,010$ mol^{-1} dm^3 cm^{-1}). These two bands are preserved in intensity and position from acidic pH values to pH 7. From pH 7 to 9, the bands experience a decrease in intensity and a slight bathocromic shift. Finally, no further changes are observed above pH 9 (see Figure 2). These spectral characteristics support the involvement of the terpyridine fragment throughout all the pH range where complexation occurs. This is an interesting feature since the polyamine would be metal-free ready to accommodate carbon dioxide with the acid Lewis assistance of the bivalent metal ion.

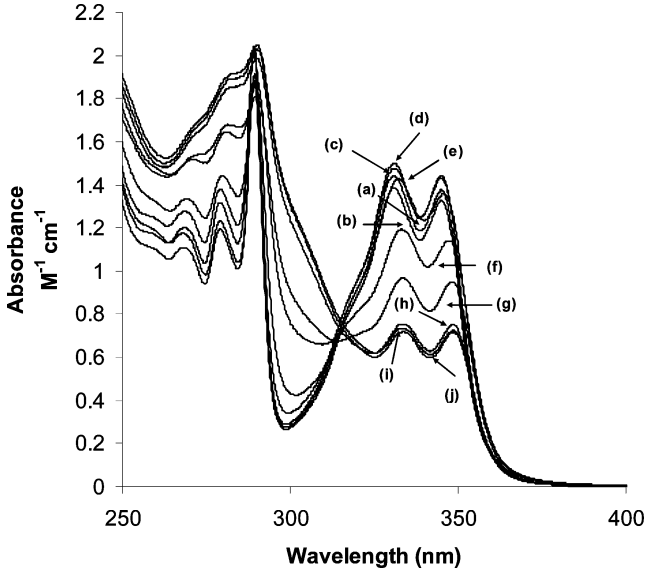

Figure 2. The pH dependence of the absorption spectra of Cu(II)/**L** in a molar ratio 1:1 M/**L**: (a) pH 2.83, (b) pH 3.16, (c) pH 4.20, (d) pH 5.05, (e) pH 5.82, (f) pH 7.15, (g) pH 8.01, (h) pH 9.04, (i) pH 9.70, (j) pH 10.20.

The distribution diagram (Figure S2, Supporting Information) shows that for a metal/ligand mole ratio 2:1 the binuclear species prevail in solution over pH 4. At neutral pH, the species existing at a larger extent are the neutral $[Cu_2L]^{2+}$ and a hydroxylated $[Cu_2L(OH)]^{+}$ denoting that hydrolysis occurs avidly with the generated OH group most likely bridging both metal ions. The stability constant of the binuclear complex formed is comparable to that of the analogous complex of the ligand **L3** containing a phenanthroline spacer.

The presence of a diprotonated binuclear $[Cu_2H_2L]^{4+}$ species means that each one of the two metal ions would be coordinated by three nitrogen atoms, one by the three pyridine nitrogens and the other one by the three central nitrogens of the polyamine bridge as it was observed in the crystal structure of the compound $[Cu_2(H_2L)(CO_3)]_2(ClO_4)_8 \cdot 9H_2O$ (vide infra). Water molecules should be completing the remaining positions of the coordination sphere of the Cu^{2+} ions. The variation with the pH of the UV−vis spectra of 2:1 solutions is analogous to that described for 1:1 Cu^{2+}/**L** solutions although two different behaviors can be individuated. Until pH 7, the bands centered at 330 and 340 nm slightly increase their absorbance on increasing the pH, while at higher pH in correspondence with the formation of the binuclear hydroxylated species there is a decrease in absorbance and a slight bathochromic shift (see Figure S3, Supporting Information). Again, the observed spectral characteristics provide unambiguous evidence for the implication

(25) Smith, R. M.; Martell, A. E. *NIST Stability Constants Database*, version 4.0; National Institute of Standards and Technology: Washington, DC, 1997.

Scheme 2

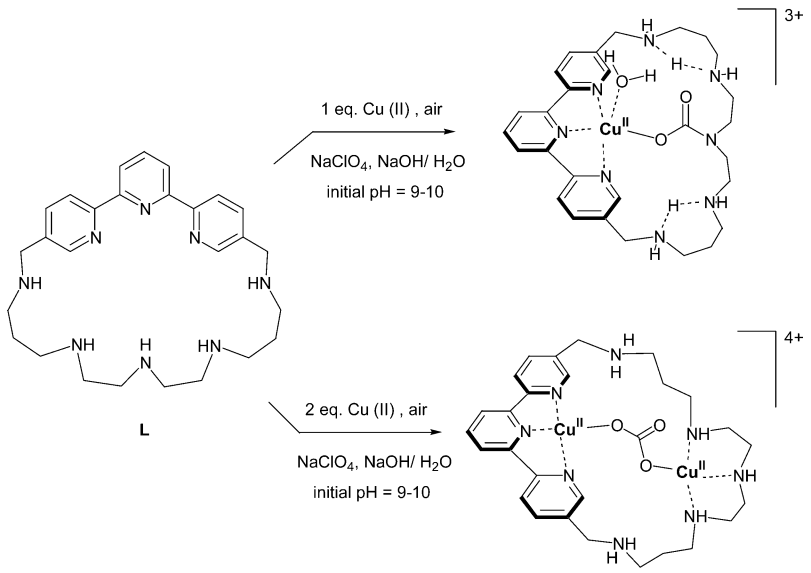

Table 4. Stability Constants for the Formation of Zn^{2+} Complexes for the Receptors **L**, **L1**, **L2**, and **L3** Determined in 0.15 M $NaClO_4$ at 298.1 K

entry	reaction	**L**	**L1**[c]	**L2**[c]	**L3**[d]
1	$M + L \leftrightarrows ML$[a]	6.9[b]	13.00(1)	14.27(1)	10.96(2)
2	$M + L + H \leftrightarrows MHL$	15.08(4)	20.43(1)		19.41(1)
3	$M + L + 2H \leftrightarrows MH_2L$	22.19(4)			26.37(1)
4	$M + L + 3H \leftrightarrows MH_3L$	28.40(6)			32.48(1)
5	$M + L + 4H \leftrightarrows MH_4L$	34.20(4)			36.43(3)
6	$ML + H \leftrightarrows MHL$	8.21(1)	7.43(1)		8.45(2)
7	$MHL + H \leftrightarrows MH_2L$	7.10(1)			6.96(1)
8	$MH_2L + H \leftrightarrows MH_3L$	6.21(2)			6.11(1)
9	$MH_3L + H \leftrightarrows MH_4L$	5.80(2)			3.95(3)
10	$M + L + H_2O \leftrightarrows ML(OH) + H$	−2.43(5)	1.88(4)		
11	$M + L + 2H_2O \leftrightarrows ML(OH)_2 + H$	−12.78(7)			
11	$ML + H_2O \leftrightarrows ML(OH) + H$	−9.31(2)	−11.12(4)		
12	$ML(OH) + H_2O \leftrightarrows ML(OH)_2 + H$	−10.35(4)			
13	$2M + L \leftrightarrows M_2L$				16.26(3)
14	$M_2L + H \leftrightarrows M_2HL$				6.28(7)
15	$2M + L + H_2O \leftrightarrows M_2L(OH) + H$	3.60(6)			8.48(4)
16	$2M + L + 2H_2O \leftrightarrows M_2L(OH)_2 + H$	−5.70(1)			−1.34(5)
17	$M_2L + H_2O \leftrightarrows M_2L(OH) + H$				−7.78(4)
18	$M_2L(OH) + H_2O \leftrightarrows M_2L(OH)_2 + H$	−9.32(6)			−9.82(5)

[a] Charges omitted. [b] Values in parentheses are standard deviations in the last significant figure. [c] Taken from ref 26. [d] Taken from ref 4.

of the terpyridine unit in the binding to the metal throughout the entire pH window of complexation.

Zn^{2+} Coordination in Aqueous Solution. The constants for the interaction of Zn^{2+} with **L** along with those for **L1**, **L2**, and **L3** are included in Table 4. The analysis of the data shows the formation of both mononuclear and binuclear Zn^{2+} complexes. At difference with Cu^{2+}, in this system the maximum degree of protonation detected for a mononuclear species was 4 instead of 5, and the hydroxylated mononuclear species $[ZnL(OH)_x]^{(2-x)+}$ with $x = -1$ and $x = -2$ were also detected at basic pH. The UV−vis spectrum at pH 3 consists of two bands centered at 320 and 330 nm whose intensity stays practically constant up to pH 7 (see Figure S4, Supporting Information). From pH 7 to 8.3, there are decreases in the intensity and bathocromic shifts of the bands. At higher pH values, there are no more apparent changes in the shape and position of the bands. Similarly to the case of Cu^{2+}, the number of mononuclear protonated species formed, the stability of the ZnL^{2+} complex (Table 4, entry 1), and the constants for its protonation steps (Table 4, entries 6−9) suggest that in these species Zn^{2+} binds at the terpyridine region occurring in all the protonation processes in nonconordinated nitrogens of the polyamine bridge.

With respect to the binuclear complexes, the only species that could be identified were the hydroxylated species $[Zn_2L(OH)_x]^{(4-x)+}$ with $x = -1$ and $x = -2$, which for Zn^{2+}/**L** mole ratios 2:1 predominate in solution above pH 7.5 (Figure S5, Supporting Information).

Carbon Dioxide Uptake. Crystal Structure of $[Cu(HL\text{-}carb)(H_2O)](ClO_4)_3 \cdot 2H_2O$. Exposure to the atmosphere of 10^{-3} M aqueous solutions of $Cu(ClO_4)_2 \cdot 6H_2O$ and **L** at an initial pH of 9 leads in a few minutes to acidification of the solution reaching a pH of ca. 6.8. After a few hours, formation of blue crystals of formula $[Cu(HL\text{-}carb)(H_2O)](ClO_4)_3 \cdot 2H_2O$ (see Scheme 2) suitable for X-ray analysis occurs. Crystals from different synthetic crops always show the same composition.

The crystals consist of the trivalent $[Cu(HL\text{-}carb)(H_2O)]^{3+}$ cation and three perchlorate anions. Cu^{2+} displays square pyramid geometry with its base defined by the three nitrogen atoms of the terpyridine fragment and an oxygen atom of the carbamate group (Figure 3). A water molecule occupies the elongated axial position of the pyramid (Table 5). The carbamate group was generated in situ by the reaction of CO_2 with the central amino group of the chain with the Lewis acid assistance of the metal ion. Therefore, in the fragment $[HL\text{-}carb]^+$, the central nitrogen of the polyamine loses one proton to form the C−N bond while two amino groups of the sides will be protonated (Scheme 2, structure 1).

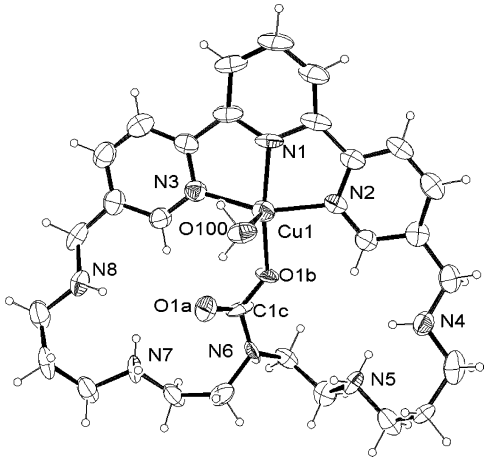

Figure 3. ORTEP drawing for the cation $[Cu(H\mathbf{L}\text{-carb})(H_2O)]^{3+}$. Thermal ellipsoids are drawn at the 25% probability level.

Table 5. Selected Distances and Angles for the Coordination Site and Carbamate Group of the $[Cu(H\mathbf{L}\text{-carb})(H_2O)]^{3+}$

	Distances (Å)		
Cu−N1	1.955(12)	Cu−O100	2.290(9)
Cu−N2	2.015(14)	C1c−O1a	1.22(3)
Cu−N3	2.034(14)	C1c−O1b	1.27(3)
Cu−O1b	1.890(12)	C1c−N6	1.39(2)
	Angles (deg)		
O1b−Cu−N1	166.2(5)	N1−Cu−O100	99.0(5)
O1b−Cu−N2	94.7(6)	N2−Cu−O100	97.5(5)
O1b−Cu−N3	104.0(6)	N3−Cu−O100	93.3(5)
O1b−Cu−O100	93.9(5)	C1c−O1b−Cu	123.5(15)
N1−Cu−N2	78.8(7)	O1a−C1c−O1b	130(2)
N1−Cu−N3	80.3(7)	O1a−C1c−N6	118(3)
N2−Cu−N3	157.8(6)	O1b−C1c−N6	112(3)

It is to be remarked that there was no need to bubble CO_2 to form this entity.[27] The angles in the carbamate moiety are close to 120°, and the C−O distance of the noncoordinated bond is shorter (C−O(1a) = 1.22 Å) than the C−O distance including the oxygen atom coordinated to the copper (C−O(1b) = 1.27 Å) (Table 5). The carbamate moiety is further stabilized by formation of a network of intramolecular hydrogen bonds involving the noncoordinated oxygen atom of carbamate, the coordinated water molecule and one of the amino groups of the chain adjacent to the central position, and the benzylic amino group of the same side of the bridge. Additionally, intramolecular hydrogen-bonding between the amino groups sharing the propylenic chains is observed at both sides of the molecule. It deserves to be emphasized that charge balance dictates that two of the amino groups of the chain are protonated since there are three perchlorate counteranions in the asymmetric unit (see Figure S6 in the Supporting Information). Although it is difficult to find out which are the protonated nitrogens in the polyamine, the arrangement of the hydrogen-bond network formed suggests

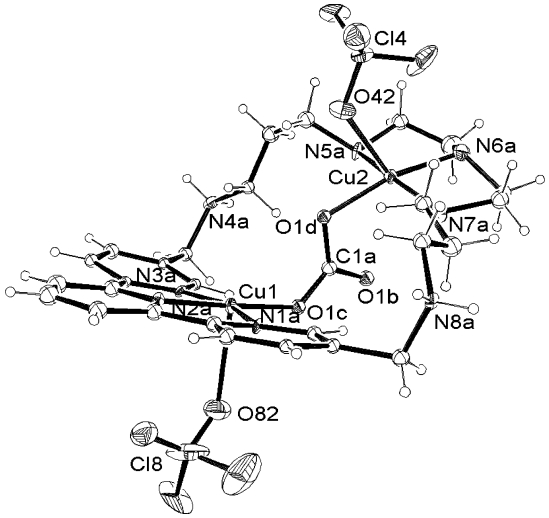

Figure 4. ORTEP drawing of one the $[Cu_2(H_2\mathbf{L})(ClO_4)_2(CO_3)]^{2+}$ units contained in the unit cell. Thermal ellipsoids are drawn at the 30% probability level.

that the amino groups closer to the central nitrogen of the chain should be protonated.

Crystal Structure of $[Cu_2(H_2L)(CO_3)]_2(ClO_4)_8\cdot 9H_2O$. The particular avidity of the Cu^{2+} complexes of **L** toward atmospheric CO_2 is also manifested in its binuclear complexes. Exposure to the atmosphere of aqueous solutions containing $Cu(ClO)_4\cdot 6H_2O$ and **L** in 2:1 mole ratio gave rise in a few hours to formation of crystals suitable for X-ray analysis of $[Cu_2(H_2\mathbf{L})(CO_3)]_2(ClO_4)_8\cdot 9H_2O$. The crystal structure consists of almost two equivalent $[Cu_2(H_2\mathbf{L})(CO_3)]^{4+}$ units, perchlorate anions, and lattice water molecules. In each unit, the Cu^{2+} bound at the terpyridine site presents strongly distorted square pyramidal geometry with the equatorial plane defined by the three pyridine nitrogens and one oxygen atom of the carbonate group which bridges both coordination sites as a μ,μ'-bismonodentate ligand (Figure 4).

The axially elongated position in this site is occupied by an oxygen atom of one of the perchlorate anions. The metal ion bounded at the polyamine site completes its equatorial plane with the three central nitrogens of the chain that share the two ethylenic chains and with the other oxygen atom coming from the μ,μ'-carbonate bridging ligand. The carbonate bridging ligand is coordinated in an anti−syn mode. Representative distances and angles of the coordination sphere are gathered in Table 6.

The squares defined by the two coordination planes form an angle of 32.2(4)° between them, and the carbonate bridging ligand defines a sort of step in a staircase connecting them. The approximate height of the step is 2 Å. Preliminary magnetic suceptibility studies show that the Cu^{2+} ions are slightly antiferromagntically coupled (Figure S7). We are currently investigating these aspects. The distance between metal ions Cu(1) and Cu(2) is 5.15 Å. The angles in the carbonate bridge are all close to 120°. Precedents to this mode of coordination of carbonate are found, for example, in the way in which carbonate is coordinated to Cu^{2+} in the mineral malaquite or in a crystal structure reported for a

(26) Unpublished results.

(27) (a) Ito, H.; Ito, T. *Bull. Chem. Soc. Jpn.* **1985**, *58*, 1755−1760. The carbamylation of a Ni^{2+} is produced by bubbling CO_2 in a solution containing the Ni^{2+} complex with the air of an external base: (b) Aresta, M.; Ballivet-Tkatchenko, D.; Dell'Amico, D. B.; Bonnet, M. C.; Boschi, D.; Calderrazzo, F.; Faure, F.; Labella, L.; Marchetti, F. *Chem. Commun*. **2000**, 1099−1100. (c) Xu, H.; Hampe, E. M.; Rudkevich, D. M. *Chem. Commun*. **2003**, 2828−2829.

Table 6. Selected Distances and Angles for the Coordination Site and Carbonate Group of the $[Cu_2(H_2\mathbf{L})(ClO_4)_2(CO_3)]^{2+}$ Units

	Distances (Å)		
Cu1−N1a	2.034(11)	Cu2−N7a	2.015(12)
Cu1−N2a	1.931(11)	Cu2−O1d	1.955(9)
Cu1−N3a	2.022 (12)	C1a− O1b	1.258(16)
Cu1−O1c	1.907(10)	C1a− O1c	1.279(16)
Cu2−N5a	2.010(12)	C1a− O1d	1.325(17)
Cu2−N6a	2.000(14)		
	Angles (deg)		
O1c−Cu1−N1a	104.3(4)	O1d−Cu2−N7a	94.0(4)
O1c−Cu1−N2a	176.2(5)	N6a−Cu2−N5a	86.1(5)
O1c−Cu1−N3a	95.6(4)	N6a−Cu2−N7a	84.0(5)
N2a−Cu1−N3a	81.3(5)	N5a−Cu2−N7a	166.1(5)
N2a−Cu1−N1a	78.9(4)	O1b−C1a−O1c	120.1(14)
N3a−Cu1−N1a	159.8(5)	O1b−C1a−O1d	119.5(14)
O1d−Cu2−N5a	93.5(4)	O1c−C1a−O1d	120.3(13)
O1d−Cu2−N6a	166.7(5)		

binuclear complex of a porphyrin-type ligand.[28,29] Analogously to the structure of the mononuclear complex, two nitrogens of the polyamine bridge are protonated that in this case should necessarily be those labeled N4a and N8a (Figure 4).

The emf Measurements on Ternary Systems. To get some light on which are the species involved in carbonate and carbon dioxide fixation by **L**, we undertook a pH-metric study on the mixed M^{2+}−**L**−carbonate systems. The measurements consisted of titrating with diluted perchloric acid solutions containing sodium carbonate, **L**·7HBr·4H_2O and $Cu(ClO_4)_2$·6H_2O or $Zn(ClO_4)_2$·6H_2O in 1:1 and 2:1 M/**L** molar ratios brought to pH 11 by the addition of NaOH. Previously, the constants for the interaction of carbonate or hydrogencarbonate with **L** and its protonated forms were determined by titrating solutions containing **L** and sodium carbonate with perchloric acid. The direct interaction of carbonate with **L** was meaningless in the absence of metal ions, and just a $[H_5\mathbf{L}\cdot HA]^{4+}$ (A = CO_3^{2-}) adduct was observed whose formation took place at a very low extent.

Interestingly, at difference with what happened in the binary system **L**−CO_3^{2-} in which CO_2 evolution was observed below pH ca. 6, when working in the presence of stoichiometric amounts of metal ions and carbonate, a much lower CO_2 evolution at acidic pH was observed which supports the carbon dioxide fixation by the complex. Table 7 gathers the cumulative and some selected stepwise formation constants derived for the interaction of the binary Cu^{2+}−**L** complexes and Zn^{2+}−**L** complexes with carbonate and its protonated forms. Figure 5 shows the distribution diagram calculated for the species existing in the system Cu^{2+}−**L**−carbonate (molar ratios 1:1:1 and 2:1:1) as a function of pH. The decomposition of the cumulative constants into stepwise ones has been done taking into account the distribution diagrams of the mixed complexes (Figure 5 and Figure S8), those for the systems M^{2+}−**L**, and the protonation constants of carbonate.[2c]

Table 7. Cumulative Stability and Selected Stepwise Formation Constants for the Systems Cu^{2+}−**L**−Carbonate and Zn^{2+}−**L**−Carbonate (**A**) Determined at 298.1 ± 0.1 K in 0.15 mol dm^{-3} $NaClO_4$

reaction[a]	M = Cu^{2+}	M = Zn^{2+}
M + 6H + **L** + **A** ⇆ MH_6**LA**	61.95(4)[b]	55.49(7)
M + 5H + **L** + **A** ⇆ MH_5**LA**	57.93(3)	51.40(6)
M + 4H + **L** + **A** ⇆ MH_4**LA**	52.39(3)	45.98(6)
M + 3H + **L** + **A** ⇆ MH_3**LA**	45.61(3)	
M + 2H + **L** + **A** ⇆ MH_2**LA**	37.84(7)	32.31(6)
M + H + **L** + **A** ⇆ MH**LA**	30.46(3)	24.62(7)
M + **L** + **A** ⇆ M**LA**	21.20(5)	15.66(8)
M + **L** + **A** ⇆ M**LA**(OH) + H	10.64(6)	5.85(8)
M + **L** + **A** ⇆ M**LA**$(OH)_2$ + 2H		−4.65(9)
2M + 4H + **L** + **A** ⇆ M_2H_4**LA**	57.84(7)	
2M + 3H + **L** + **A** ⇆ M_2H_3**LA**	53.2(9)	
2M + 2H + **L** + **A** ⇆ M_2H_2**LA**	48.52(5)	
2M + H + **L** + **A** ⇆ M_2H**LA**	42.33(9)	29.1(1)
2M + **L** + **A** ⇆ M_2**LA**	35.43(9)	22.1(1)
2M + **L** + **A** ⇆ M_2**LA**(OH) + H	28.17(8)	14.69(8)
2M + **L** + **A** ⇆ M_2**LA**$(OH)_2$ + 2H		5.2(1)
2M + **L** + **A** ⇆ M_2**LA**$(OH)_3$ + 3H		−5.4(1)
MH_4**L** + H_2**A** ⇆ MH_6**LA**	4.3[c]	5.2
MH_3**L** + H2**A** ⇆ MH_5**LA**	5.7	6.9
MH_3**L** + H**A** ⇆ MH_4**LA**	6.5	7.8
MH_2**L** + H**A** ⇆ MH_3**LA**	5.9	
MH**L** + H**A** ⇆ MH_2**LA**	5.5	7.4
M**L** + H**A** ⇆ MH**LA**		7.9
M**L** + **A** ⇆ M**LA**		8.8
M**L**(OH) + **A** ⇆ M**LA**(OH)		8.3
M**L**$(OH)_2$ + **A** ⇆ M**LA**(OH)		8.1
M_2H_2**L** + H_2**A** ⇆ M_2H_4**LA**	4.8	
M_2H**L** + H_2**A** ⇆ M_2H_3**LA**	5.5	
M_2H**L** + H**A** ⇆ M_2H_2**LA**	7.1	
M_2**L** + H**A** ⇆ M_2H**LA**	7.3	
M_2**L**(OH) + H_2**A** ⇆ M_2H**LA**		9.4
M_2**L**(OH) + H**A** ⇆ M_2**LA**	7.2	8.6

[a] Charges omitted. [b] Values in parentheses are standard deviations in the last significant figure. [c] Errors omitted.

As seen in Figure 5, the mixed species form quantitatively above pH 6 for the two metal ions and for both 1:1:1 and 2:1:1 M/**L**/A molar ratios, the constants for the formation of the Zn^{2+}−**L**−carbonate adducts being higher than those for the Cu^{2+}−**L**−carbonate adducts. Below pH 6, in correspondence with the second protonation of carbonate, there is a decrease in the amount of complexed carbonate which is more pronounced in the case of Cu^{2+}.

In relation with the preparation of the crystal structures, it is interesting to remark that the stoichiometries of the crystals obtained from 1:1 and 2:1 Cu^{2+}−**L** solutions by fixation of atmospheric CO_2 correspond to species existing in 1:1:1 and 2:1:1 Cu^{2+}−**L**−carbonate solutions at pH ca. 6.8, which is the final pH of the solution from which the crystals evolve. For 1:1:1 Cu^{2+}−**L**−carbonate mole ratio, at this pH the species present in solution would be $[CuH_4\mathbf{L}A]^{4+}$, $[CuH_3\mathbf{L}A]^{3+}$, and $[CuH_2\mathbf{L}A]^{2+}$ with percentages of 42% for the first two species and only of 4% for the last one. From these, the tricharged species is the one which

(28) (a) Healy, P. C.; White, A. H. *J. Chem. Soc., Dalton Trans.* **1972**, *17*, 1913−1972. (b) Van den Brenk, A. L.; Byriel, K. A.; Fairlie, D. P.; Gaban, L. R.; Hanson, G. R.; Hawkins, C. J.; Jones, A.; Kennard, C. H. L.; Moubaraki, B.; Murray, K. S. *Inorg. Chem.* **1994**, *33*, 3549−3557.

(29) Several examples of carbonato bridged metal complexes are described in the following: (a) Kolks, G.; Lippard, S. J.; Waszczak, J. V. *J. Am. Chem. Soc*. **1980**, *102*, 4832−4833. (b) Kitajima, N.; Hikichi, S.; Tanka, M.; Moro-oka, M. *J. Am. Chem. Soc*. **1993**, *115*, 5496−5508. (c) Bazzicalupi, C.; Bencini, A.; Bencini, A.; Bianchi, A.; Corana, F.; Fusi, V.; Giorgi, C.; Paoli, P.; Paoletti, P.; Valtancoli, B.; Zanchini, C. *Inorg. Chem*. **1996**, *35*, 5540−5548. (d) Escuer, A.; Mautner, F. A.; Peñalba, E.; Vicente, R. *Inorg. Chem.* **1998**, *37*, 4190−4196. For reviews on related topics, see the following: (e) Walther, D.; Ruben, M.; Rau, S. *Coord. Chem. Rev.* **1999**, *182*, 67−100. (f) Newell, R.; Appel, A.; DuBois D. L.; Rakowski DuBois, M. *Inorg. Chem*. **2005**, *44*, 365−373.

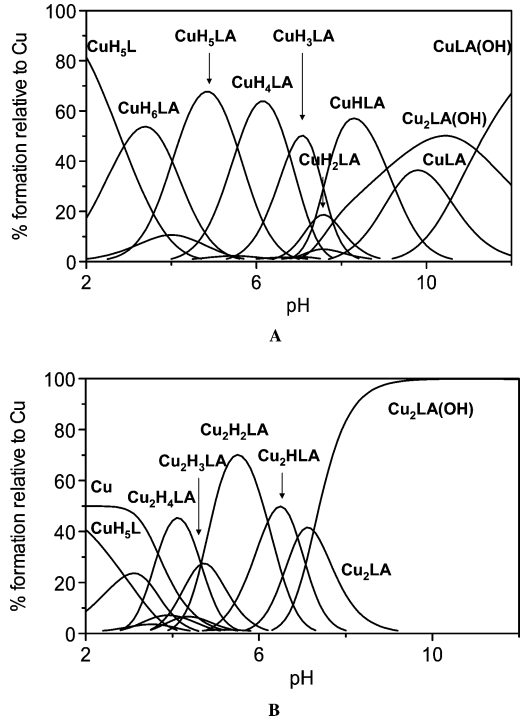

Figure 5. Distribution diagrams for the ternary system $Cu^{2+}-\mathbf{L}-$carbonate: (A) $[Cu^{2+}] = [\mathbf{L}] = [A] = 10^{-3}$ M; (B) $[Cu^{2+}] = 2 \times 10^{-3}$ M, $[\mathbf{L}] = [A] = 10^{-3}$ M.

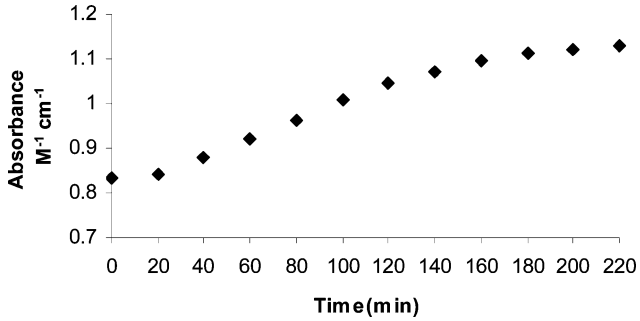

Figure 6. Evolution with time of the maximum of the band at 340 nm.

precipitates (Scheme 2). For 2:1:1 $Cu^{2+}-\mathbf{L}-$carbonate mole ratio the species existing in solution are $[Cu_2H_2\mathbf{L}A]^{4+}$(15%), $[CuH_3\mathbf{L}A]^{3+}$ (47%), and $[CuH_2\mathbf{L}A]^{2+}$ (30%) from which the first one is the one we have isolated.

UV−Visible Spectroscopy. CO_2 uptake has also been followed recording the evolution with time of the UV−vis spectra of magnetically stirred solutions exposed to the atmosphere containing either Cu^{2+} or Zn^{2+} and **L** in molar ratio 1:1 at pH 8.7. CO_2 capture yields a decrease in pH due, among other factors, to the reaction

$$CO_2 + R_2NH = R_2NCOO^- + H^+ \qquad (1)$$

Thus, the spectral changes are those brought about by an acidification of the system, namely, a slight increase of the intensity of the bands (see Figure S9, Supporting Information). The final pH attained by the solution was 6.70. A plot of the absorbance at 330 nm against time shows a continuous increase in the absorbance until a plateau is reached after 120 min of exposure (Figure 6). Unfortunately, for solutions with a 2:1 Cu^{2+}/**L** mole ratio, the changes observed in the

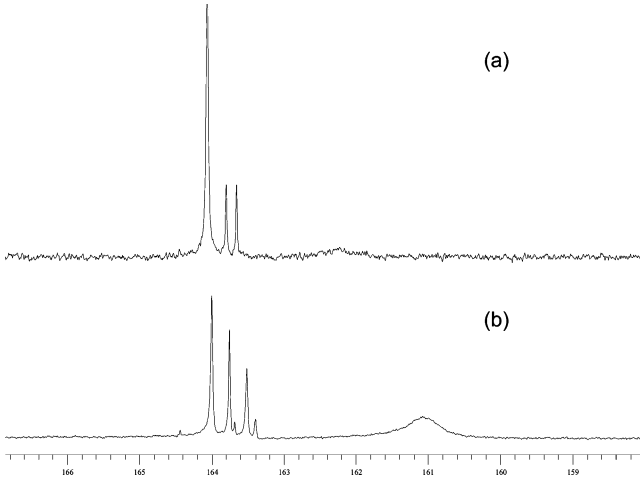

Figure 7. (a) ^{13}C NMR for Zn^{2+}/**L**/$NaH^{13}CO_3$ at molar ratio M/**L**/A 1:1:1, pD = 7.0; (b) ^{13}C NMR for Zn^{2+}/**L**/$NaH^{13}CO_3$ at molar ratio M/**L**/A 1:1:3, pD = 7.0.

spectra are not so significant preventing a straightforward analysis of the system. A plausible explanation can be that for this metal/ligand ratio CO_2 is fixed as carbonate and the characteristic ligand to metal charge transfer (LMCT) appears at 349 nm overlapped with the terpyridine bands minimizing the changes.[30]

For the system Zn^{2+}/**L** in 1:1 mole ratio at pH 8.6, similarly to the analogous Cu^{2+}/**L** system, addition of CO_2 yields an acidification of the system and a progressive increase in the absorbance of the spectra. A plot of the maximum absorbance against time yields a curve with a profile similar to that of Cu^{2+} and a saturation time of ca. 90 min (see Figures S10 and S11, Supporting Information).

NMR Studies and MSI Spectroscopy. Although we have not yet obtained crystals of ternary $Zn-\mathbf{L}-$carbonate complexes suitable for X-ray analysis, ^{13}C NMR spectra of samples in which enriched $NaH^{13}CO_3$ has been added to solutions containing **L** and Zn^{2+} at an appropriate pH provide valuable information.

Samples containing Zn^{2+}/**L**/$NaH^{13}CO_3$ in 1:1:1 or 1:1:3 mole ratios at pD = 7.0 provided the spectra shown in Figure 7 in which there is a very intense signal at 163.9 ppm and another two at 163.7 and 163.5 ppm. Additionally, the spectra of the 1:1:3 samples show a broader signal at 161.8 ppm that can be ascribed to free hydrogen carbonate. Also in this sample, the signal corresponding to the CO_2 dissolved in water appears at 120 ppm. The three signals at ca. 163 ppm can be attributed to different forms of carbon dioxide, carbamate, or carbonate coordination to the metal ion. Two-dimensional $^1H-^{13}C$ HMBC NMR experiments show a cross-peak between the most intense ^{13}C signal and the protons of one of the methylene groups of the central part of the chain supporting the formation of the carbamate unit (see Figure S12, Supporting Information).

MSI spectroscopy also provides evidence for the formation of the carbamate group in the 1:1 complexes. The peak at *m*/*z* 581.3 recorded in the spectra without fragmentation and

(30) Kitajima, N.; Fujisawa, K.; Koda, T.; Hikichi, S.; Moro-oka, Y. *J. Chem. Soc., Chem. Commun.* **1990**, 1357−1358.

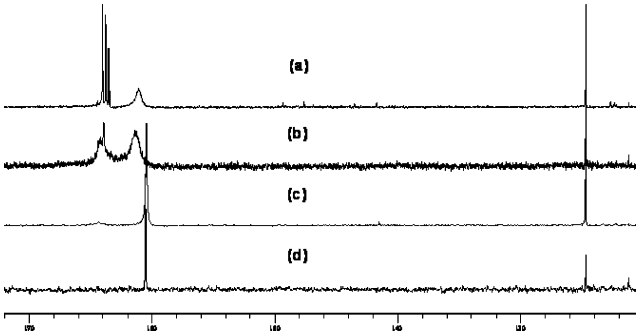

Figure 8. NMR spectra for the system M/**L**/A in 1:1:3 molar ratio at pD = 7, T = 298.1 K: (a) Zn^{2+} + **L** + $NaH^{13}CO_3$; (b) Zn^{2+} + **L3** + $NaH^{13}CO_3$; (c) Zn^{2+} + **L2** + $NaH^{13}CO_3$; (d) Zn^{2+} + **L1** + $NaH^{13}CO_3$.

the isotopical distribution shown in Figure S13 which coincides with the theoretical one support the formation of the carbamate moiety in the 1:1 complex. The peaks at *m*/*z* 537.4 and 475.5 can be attributed to the loss of CO_2 and of CO_2 and metal, respectively. In the spectra recorded with fragmentation, the two latter peaks can be also observed (see Figure S14, Supporting Information).

On the other hand, we have recorded the evolution with time of the ^{13}C NMR spectra of Zn^{2+}/**L** solutions at pD = 8.7 in 1:1 mole ratio after addition of an equimolar amount of enriched $NaH^{13}CO_3$. The signal of free carbonate at 161.8 ppm can be appreciated in the spectra only for times below 10 min after the addition of sodium hydrogencarbonate. Afterward that signal disappears and only the three signals at around 163 ppm are present which do not bear any further evolution after 20 h (see Figure S15, Supporting Information).

To compare the behavior of **L** with the other ligands containing the same polyamine unit, we have recorded the corresponding spectra of **L**, **L1**, **L2**, and **L3** under the same experimental conditions (Figure 8). Interestingly enough, in the case of the pyridinophane **L2**, no signals corresponding to Zn**L**−carbonate complexes were detected. As seen in the crystal structure of the Cu^{2+} complex of the same ligand,[3] in this compound the bridge has enough flexibility to wrap around the metal ion fulfilling its coordination sphere and preventing the uptake of further substrates or ligands. An NMR analysis shows that a similar situation occurs for Zn^{2+}.[26]

A similar situation occurs for the open-chain polyamine **L1** in which the signals at 125 and 161 ppm attributable to free-CO_2 and free-carbonate, respectively, are predominant in solution. The phenanthrolinophane **L3** shows an intermediate situation. In this case, although the signal at ca. 163 ppm starts to be intense, there is still an intense remnant signal at 161 ppm attributable to noncoordinated carbonate. Therefore, all these spectral data suggest that the combination of the 5,5″-terpyridine fragment and this particular pentaamine is very appropriate for achieving a high degree of carbonate fixation.

Electrochemical Response. A typical SQWV of Cu^{2+}-receptor binary solutions is depicted in Figure 9a, corresponding to a 2.8×10^{-4} M Cu^{2+} plus 3×10^{-4} M **L** solution at pH 5.5. On scanning the potential in the negative direction,

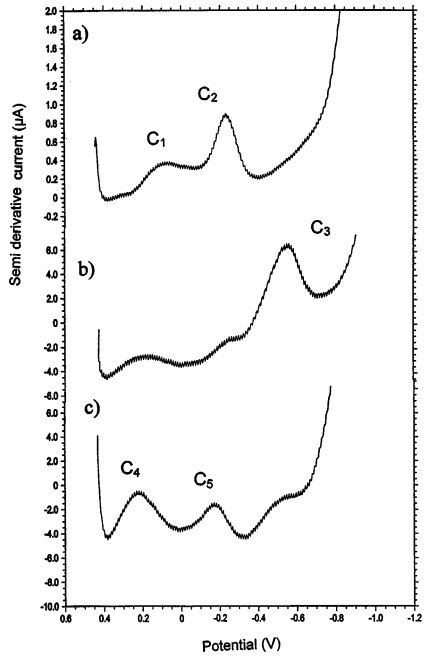

Figure 9. Semiderivative convolution of SQWVs at a gold electrode of a 2.8×10^{-4} M Cu^{2+} plus 3×10^{-4} M **L** solution in 0.15 M $NaClO_4$ at pH 5.5: (a) degasified solution; (b) same conditions, after 6 h of exposure to the air and subsequent Ar bubbling; (c) same conditions, third scan. The potential step increment is 4 mV, square wave amplitude is 25 mV, and the frequency is 15 Hz.

two peaks at +0.13 (C_1) and −0.20 V (C_2) appear, as can be seen in Figure 9a. This response can be interpreted in terms of two successive one-electron processes forming successively a Cu^+−**L** complex and Cu metal. The electrochemical process involves a comproportionation reaction between the deposited Cu^0 and the parent Cu^{2+}−**L** complex, resulting in an enhancement of the second voltammetric peak at the expense of the first one. Consistently with that scheme, the peak C_2 is enhanced at the expense of the peak C_1 on decreasing the square wave frequency.

As the pH is increased, the voltammetric profile remains essentially unchanged. The peak potentials shift slightly toward more negative potentials until they remain constant and equal to +0.02 and −0.40 V above pH 6.5. As the potential is cycled between +0.45 and −0.65 V, EQCM provided frequency/potential graphs similar to those obtained at a reference $Cu(ClO_4)_2$ + $HClO_4$ solution, denoting that copper metal is deposited and oxidatively redissolved during electrochemical turnovers.[16]

The voltammetric response of solutions containing Cu^{2+} and **L** changes progressively under exposure to the atmosphere. As shown in the SQWV depicted in Figure 9b, after prolonged exposure to air, a unique reduction peak at −0.55 V (C_3) appears. This peak is negatively shifted on bubbling CO_2 through the solution, denoting that carbon dioxide participates in metal coordination. Upon repetitive scanning of the potential, peak C3 decreases whereas two new cathodic peaks at +0.22 (C_4) and −0.17 (C_5) V appear, as shown in Figure 9c. Such peaks can be attributed to the stepwise reduction of $Cu(CO)^+$ complexes formed as a result of the formation of CO at potentials of ca. −1.0. [31]

The voltammetric response observed in ternary solutions can be rationalized by taking into account prior data on the relative stability of the Cu^{2+} and Cu^{+} complexes with polyammonium receptors. As previously described for the Cu^{2+}-2,6,9,13-tetraaza[14]paracyclophane system,[32] binary metal-macrocyclic receptor complexes stabilize the intermediate Cu^{+} oxidation state toward disproportionation into Cu^{2+} and Cu^{0}. Apart from solvation and electronic factors, this stabilization arises as a result of the disposal of vacant coordination sites enabling the Cu^{+} ion to adopt its preferred tetrahedral or pseudotetrahedral coordination. The introduction of an axial ligand blocks this possibility and destabilizes Cu^{+} complexes.

In the system studied here, the Cu^{2+} center in the complex $[Cu(H\mathbf{L}\text{-carb})(H_2O)]^{3+}$ possesses a square pyramidal geometry: the base of the pyramid is constituted by three pyridinic nitrogens and one oxygen atom of the carbamate group. The distorted axial position is occupied by a water molecule. Although one can expect that the axial water molecule might easily be removed in order to adopt a tetrahedral configuration, the rigidity introduced by the carbamate group, that is coordinated to one of the amino groups adjacent to the central position through a hydrogen bond, presumably blocks such tetrahedral configuration. As a result, the intermediate Cu^{+} oxidation state is destabilized. Accordingly, the peak C_3 in Figure 9b can be represented as a two-electron process:

$$[Cu(H\mathbf{L}\text{-carb})(H_2O)]^{3+} + H^{+} + 2e^{-} \rightarrow Cu^{0} + H_2\mathbf{L}^{2+} + H_2O + CO_2 \quad (2)$$

The voltammetric response of Zn^{2+}-receptor solutions was also significantly modified upon exposure to CO_2. At pH values between 5 and 7, binary $Zn^{2+}-\mathbf{L}$ complexes are reduced via a two-electron process at a potential of -1.38 V. After exposure to air, an additional peak at -1.42 V appears and increases progressively. EQCM data indicated that a deposit of zinc metal is formed in all cases at potentials more negative than -1.4 V. This behavior denotes the formation of ternary $Zn^{2+}-\mathbf{L}-$carbonate complexes whose electrochemical reduction parallels that represented by eq 2.

Electrochemical CO_2 Activation. Figure 10 compares the cyclic voltammetric curves at the glassy-carbon electrode of (a) a CO_2-saturated solution containing Cu^{2+} (0.5 mM) and **L** (0.5 mM) at pH 5.0, (b) a pristine CO_2-saturated aqueous solution, and (c) a solution containing Cu^{2+} (0.5 mM) and **L** (0.5 mM) at pH 5.0 in the absence of CO_2. In the absence of the complex, a modest increase in the current appears at potentials ca. -1.1 V (Figure 10b). In the presence of the complex, however, the current at those potentials is significantly enhanced (Figure 10a). This current increase must be attributed to the reduction of carbon dioxide rather than a catalytic effect on background proton reduction since CVs of Cu^{2+} plus **L** solutions do not provide enhanced currents (Figure 10c) in the absence of CO_2.

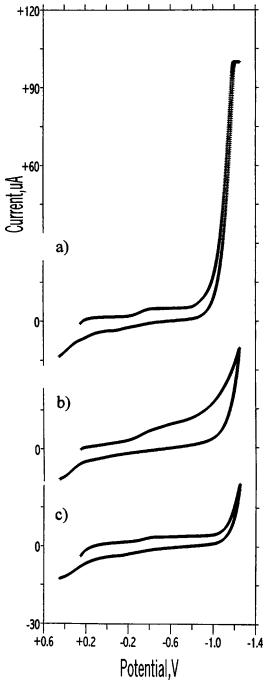

Figure 10. CVs at a GCE of (a) CO_2-saturated solution containing Cu^{2+} (0.5 mM) and **L** (0.5 mM) at pH 5.0, (b) a pristine CO_2-saturated aqueous solution, and (c) a solution containing Cu^{2+} (0.5 mM) and **L** (0.5 mM) at pH 5.0 in the absence of CO_2. The electrolyte is $NaClO_4$ 0.15 M; the potential scan rate is 100 mV/s.

The reduction of carbon dioxide at inert electrodes proceeds through the mechanism suggested by Amatore and Saveant in which carbon monoxide, carbonate, and oxalate ions can be formed through disproportionation or dimerization of the anion radical produced in the initial one-electron reduction of carbon dioxide,[33] CO being by far the main reduction product in aqueous solution.[34,35]

In the case of the $Zn^{2+}-\mathbf{L}$ system, the reduction of the complex occurs at a potential close to that for the direct, uncatalyzed reduction of CO_2. Then, a single outer-sphere catalytic mechanism involving a well-known reduction/regeneration scheme can be proposed. In the case of the $Cu^{2+}-\mathbf{L}$ system, however, since the catalytic reduction potential of CO_2 is significantly more negative than the formal reduction potential of the catalyst, a simple outer-sphere electron transfer between the copper complex and carbon dioxide is not likely because no reduction of CO_2 occurs at potentials at which the reduction of the complex occurs. Thus, an inner-sphere pathway involving the formation of ternary $Cu^{+}-\mathbf{L}-CO_2$ complexes seems called for, so that CO_2 reduction presumably occurs at a potential corresponding to the redox potential of an adduct formed between the reduced substrate and the catalyst.[36−40]

(31) Richard, P.; Warburton, G.; Wu, W.; Kuwana, T.; Busch, D. H. *Anal. Chem.* **1991**, *63*, 2772−2777.
(32) Doménech, A.; García-España, E.; Luis, S. V.; Marcelino, V.; Miravet, J. F. *Inorg. Chim. Acta* **2000**, *299*, 238−246.
(33) Amatore, C.; Saveant, J.-M. *J. Am. Chem. Soc.* **1981**, *103*, 5021−5023.
(34) Beley, M.; Collin, J. P.; Ruppert, R.; Sauvage, J. P. *J. Chem. Soc., Chem. Commun.* **1984**, 1315−1316.
(35) Beley, M.; Collin, J. P.; Ruppert, R.; Sauvage, J. P. *J. Am. Chem. Soc.* **1986**, *108*, 7461−7467.
(36) Lei, Y.; Anson, F. C. *Inorg. Chem.* **1994**, *33*, 5003−5009.
(37) Ogura, K.; Ishikawa, H. *J. Chem. Soc., Faraday Trans.* **1984**, *180*, 2243−2253.
(38) Barley, M. H.; Takeuchi, K.; Murphy, W. R.; Meyer, T. J. *J. Chem. Soc., Chem. Commun.* **1985**, 507−508.

The activation of CO_2 by effect of coordination with the studied copper complexes was tested by studying the voltammetry of solutions of ascorbic acid. In the presence of concentrations of Cu^{2+}−**L** ca. 10^{-5} M, the potential for the electrochemical oxidation of ascorbic acid in concentration 2×10^{-3} M in CO_2-saturated solutions at pH between 5 and 7 is lowered ca. 300 mV (see Figure S16, Supporting Information). The oxidation product is irreversibly oxidized at −0.95 V, suggesting that the addition of CO_2 to anionic forms of ascorbate is catalytically prompted by complex formation with Cu^{2+}−**L**, following a scheme similar to that proposed by Appel et al. for the electrochemical concentration of carbon dioxide mediated by different Cu^{2+} complexes with tetraazacyclotetradecane macrocycles using 2,6-di-*tert*-butyl-benzoquinone as the redox-active carrier.[41]

Conclusions

The chemistry of the Cu^{2+} and Zn^{2+} complexes of a novel terpyridinophane (**L**) able to fix CO_2 in a way reminiscent to the enzyme rubisco is discussed and presented. The crystal structure of the complex $[Cu(H_2\mathbf{L})(H_2O)(carb)](ClO_4)_3 \cdot 2H_2O$ shows how carbon dioxide was fixed forming a carbamate bond which was stabilized by interaction with the metal ion and by formation of an intramolecular network of hydrogen bonds. The features of this CO_2 fixation are similar to the main characteristics of the rubisco active site. In the case of the 2:1 Cu^{2+}/**L** complex, CO_2 fixation occurs as a carbonate bridging μ,μ'-bis(monodentate) ligand between the metal ions. The pH-metric titrations on the ternary Cu^{2+}/**L**/carbonate and Zn^{2+}/**L**/carbonate systems show quantitative formation of mixed complexes above pH 6. The stoichiometries of the predominant ternary complexes formed in solution at pH = 6.8 agree with those of the crystalline compounds. In the case of Zn^{2+}, carbamate fixation has been evidenced by UV−vis spectroscopy, NMR, and ESI techniques. The take up time of CO_2 compares well with previously described systems. All these data together with the reduction in the overpotential of the CO_2 reduction are very appealing for developing systems for CO_2 reutilization. We are currently studying these aspects.

Acknowledgment. The authors want to thank the referees for their helpful comments and suggestions. Financial support from DGICYT Project BQU2003-09215-CO3-01 (Spain) is gratefully acknowledged. P.G. and J.M.Ll. thank MCYT of Spain for a Ramón y Cajal contract. B.V. thanks Ayuntamiento de Valencia for a "Carmen y Severo Ochoa" grant.

Supporting Information Available: Figure S1, distribution diagram for the system H^+−**L**; Figure S2, distribution diagram for the system Cu^{2+}−**L**; Figure S3, distribution diagram for the system Zn^{2+}−**L**; Figure S4, pH dependence of the absorption spectra of Cu^{2+}/**L** in a molar ratio 2:1 M/**L**; Figure S5, pH dependence of the absorption spectra of Zn^{2+}/**L** in a molar ratio 1:1 M/**L**; Figure S6, Pluto representation showing the contents of the asymmetric unit of **1**; Figure S7, $X_M T$ versus T for compound **2**; Figure S8, distribution diagrams for the ternary system Zn^{2+}−**L**−carbonate; Figure S9, electronic spectral change in the reaction of Cu^{2+}/**L** with atmospheric CO_2; Figure S10, electronic spectral change in the reaction of Zn^{2+}/**L** with atmospheric CO_2; Figure S11, evolution with time of the maximum of the band at 330 nm for Zn^{2+}/**L**; Figure S12, $^1H-^{13}C$ HMBC NMR of a solution containing enriched $NaH^{13}CO_3$, Zn^{2+}, and **L** in molar ratio 1:1:3 at pD = 7.0; Figure S13, (a) ESI spectra without fragmentation for Zn^{2+}/**L**/carbamate, (b) theoretic isotopical distribution for Zn^{2+}/**L**/carbamate, (c) isotopical distribution for Zn^{2+}/**L**/carbamate; Figure S14, ESI spectra recorded with fragmentation for Zn^{2+}/**L**/carbamate; Figure S15, ^{13}C NMR evolution for Zn^{2+}/**L**/$NaH^{13}CO_3$ at molar ratio M/**L**/A 1:1:1, pD = 8.7; Figure S16, CVs of a 2×10^{-3} M solution of ascorbic acid in 0.10 M $NaClO_4$ at pH 5.0, (a) pristine solution, (b) CO_2-saturated solution, (c) same conditions, plus Cu^{2+}/**L** 10^{-4} M, and two crystallographic data files in CIF format. This material is available free of charge via the Internet at http://pubs.acs.org.

IC060278D

(39) (a) Toth, J. E.; Anson, F. C. *J. Am. Chem. Soc*. **1989**, *111*, 2444−2451. (b) Rhodes, M. R.; Barley, M. H.; Meyer, T. J. *Inorg. Chem*. **1991**, *30*, 629−635.

(40) Hayon, J.; Raveh, A.; Bettelheim, A. *J. Electroanal. Chem*. **1993**, *359*, 209−221.

(41) Appel, A. M.; Newell, R.; DuBois, D. L.; DuBois, M. *Inorg. Chem*. **2005**, *44*, 3046.